ChemPubSoc Europe

DOI: 10.1002/cphc.201301047

Carbon-Double-Bond-Free Printed Solar Cells from $TiO_2/CH_3NH_3PbI_3/CuSCN/Au$: Structural Control and Photoaging Effects

Seigo Ito,*[a] Soichiro Tanaka,[a] Henri Vahlman,[b] Hitoshi Nishino,[c] Kyohei Manabe,[c] and Peter Lund[b]

Carbon double bond-free printed solar cells have been fabricated with the structure <F-doped SnO_2 (FTO)/dense TiO_2/nanocrystalline $TiO_2/CH_3NH_3PbI_3/Au$> and <FTO/dense TiO_2/nanocrystalline $TiO_2/CH_3NH_3PbI_3/CuSCN/Au$>, in which CuSCN acts as a hole conductor. The thickness of the $CH_3NH_3PbI_3$ layer is controlled by a hot air flow during spin coating. The best conversion efficiency (4.86%) is obtained with <FTO/dense TiO_2/nanocrystalline TiO_2/thin $CH_3NH_3PbI_3$ (hot-air dried)/CuSCN/Au>. However, a thick $CH_3NH_3PbI_3$ layer on CuSCN is better for light-exposure stability (100 mW cm^{-2} AM 1.5) when not encapsulated. Without the CuSCN coverage, the black $CH_3NH_3PbI_3$ crystal changes to yellow during the light-exposure stability test, which is due to the transformation of the $CH_3NH_3PbI_3$ perovskite crystal into hexagonal PbI_2.

1. Introduction

Solar cells require three important characteristics to be cost-effective power generation systems: a high efficiency, a high stability, and a low price. However, a cost-effective photovoltaic system has not yet been developed. The fabrication of low-cost solar cells requires non-vacuum methods, such as screen printing, spray deposition, spin coating, and electrochemical deposition.

To achieve a high stability with printed solar cells, the carbon double bond (C=C) should be eliminated due to the cleavage of this bond under light irradiation.[1] We have previously fabricated carbon double bond-free printed solid-state solar cells by using inorganic materials on nanocrystalline TiO_2 electrodes.[2–5] The best conversion efficiency (5.7%) was obtained with a cell structure of <F-doped SnO_2 (FTO)/dense TiO_2/nanocrystalline $TiO_2/Sn_2S_3/CuSCN/Au$>, which is referred to as an extremely thin absorber (ETA) solar cell.[3]

Since 2012 solid-state printed solar cells with carbon double bond materials have been reported with high efficiencies of 9.7–15.0% using perovskite $CH_3NH_3PbX_3$ (X: halide) as a photoabsorber.[6–9] The $CH_3NH_3PbX_3$ solar cell contains organic hole conductors that have carbon double bonds, such as 2,2′,7,7′-tetrakis-(*N*,*N*-di-*p*-methoxyphenylamine)-9,9′-spirobifluorene (spiro-OMe-TAD) or poly-triarylamine (PTAA). If the organic hole conductor could be changed to CuSCN to form an inorganic printed solar cell, then the device would be a carbon double bond-free printed device.

In this study, carbon double bond-free (inorganic) printed solar cells with the structure <FTO/dense TiO_2/nanocrystalline $TiO_2/CH_3NH_3PbI_3/CuSCN/Au$> have been fabricated for the first time. This article covers three topics: 1) a new hole-transporting material (CuSCN) for $CH_3NH_3PbI_3$ solar cells, 2) the structure control of $CH_3NH_3PbI_3$ solar cells with CuSCN, and 3) the stability testing of $CH_3NH_3PbI_3$ solar cells with CuSCN. Each topic is related to the others. The $CH_3NH_3PbI_3$ structure was controlled by hot-air drying during spin coating (Figure 1). The variation

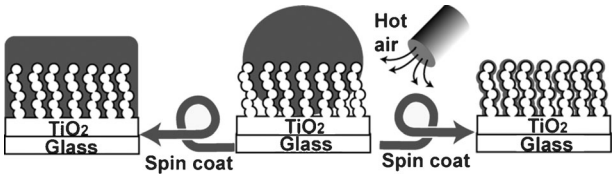

Figure 1. Spin-coating method with or without hot air flow.

of the $CH_3NH_3PbI_3$ structure influences not only the photovoltaic effect, but also the stability. Although solar cells with perovskite $CH_3NH_3PbX_3$ fabricated using low-cost processes (spin coating) have high efficiencies, their stability has been ambiguous. Kim et al. and Noh et al. have reported stable efficiencies for perovskite $CH_3NH_3PbX_3$ solar cells without encapsulation stored in the dark.[6,8] Burschka et al. encapsulated perovskite $CH_3NH_3PbX_3$ solar cells under argon and conducted durability

[a] *Prof. S. Ito, S. Tanaka*
Department of Electric Engineering and Computer Science
Graduate School of Engineering
University of Hyogo
2167 Shosha, Himeji, Hyogo 671-2280 (Japan)
Fax: (+81) 79-267-4858
E-mail: itou@eng.u-hyogo.ac.jp

[b] *H. Vahlman, Prof. P. Lund*
New Energy Technologies Group
Department of Applied Physics
Aalto University
P.O. Box 14100, 00076 Aalto, Espoo (Finland)

[c] *H. Nishino, K. Manabe*
Energy Technology Laboratories
Osaka Gas Co., Ltd.
6-19-9 Konohana-Ku, Osaka 554-0051 (Japan)

tests under constant illumination at approximately 100 mW cm^{-2} and 45 °C.[9] These cells exhibited promising long-term stability, with the conversion efficiency of the photovoltaic device maintaining more than 80% of its initial value after a period of 500 h. However, the sealing of the organic materials against water and oxygen cannot be perfect; therefore, it is important to evaluate the stability under light irradiation without encapsulation. In this work, we investigated the stability of the perovskite $CH_3NH_3PbI_3$ under 1 Sun irradiation (air mass (AM) 1.5) without encapsulation. The perovskite $CH_3NH_3PbI_3$ solar cells can function without a hole-transport material;[10] therefore, the photovoltaic effect and stability were evaluated with and without an inorganic hole-transport material (CuSCN).

2. Results and Discussion

The thickness of $CH_3NH_3PbI_3$ deposited by spin coating can be controlled by using a hot air flow, as shown in Figure 1. Figure 2 shows cross-sectional scanning electron microscopy (SEM) images of $CH_3NH_3PbI_3$ layers on the nanocrystalline TiO_2 electrodes. Without the hot air flow, the $CH_3NH_3PbI_3$ coated onto the nanocrystalline TiO_2 was approximately 1 μm thick, whereas with hot-air drying, no additional layer was observed on the nanocrystalline TiO_2 layer, and $CH_3NH_3PbI_3$ was only deposited inside the TiO_2 pores.

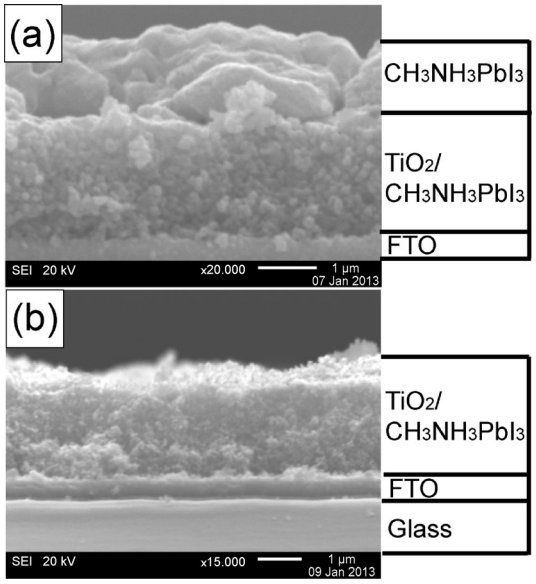

Figure 2. Cross-sectional SEM images of nanocrystalline $TiO_2/CH_3NH_3PbI_3$ layers deposited on FTO/glass substrate (without compact TiO_2 layer) by spin coating a) with or b) without hot-air drying. Each scale bar represents 1 μm.

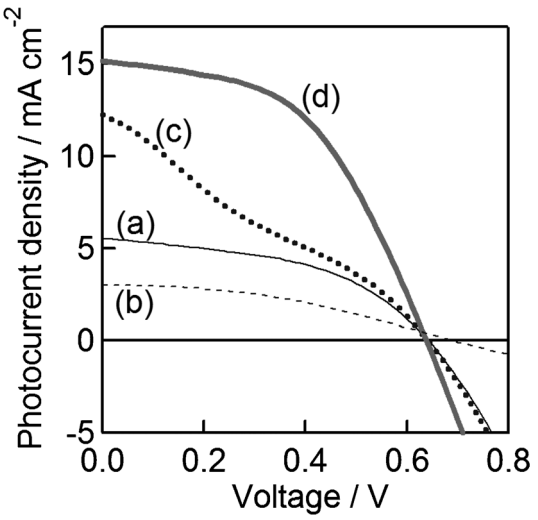

Figure 3. Current–voltage (*I–V*) curves for solar cells with the best conversion efficiencies: line a) < FTO/TiO_2/$CH_3NH_3PbI_3$ (without hot-air drying)/Au >; b) < FTO/TiO_2/$CH_3NH_3PbI_3$ (with hot-air drying)/Au >; c) < FTO/TiO_2/$CH_3NH_3PbI_3$ (without hot-air drying)/CuSCN/Au >; d) < FTO/TiO_2/$CH_3NH_3PbI_3$ (with hot-air drying)/CuSCN/Au >.

Solar cells were fabricated using the $CH_3NH_3PbI_3$ layer spin-coated on the nanocrystalline TiO_2 with/without hot-air drying and with/without an inorganic hole conductor (CuSCN) by printing (doctor blade process). The photovoltaic characteristics of the solar cells (average of three cells) are summarized in Table 1. The best results were obtained with hot-air drying during spin coating of the $CH_3NH_3PbI_3$ layer and with the addition of CuSCN: 15.2 mA cm^{-2} short-circuit photocurrent density (J_{SC}), 0.64 V open-circuit photovoltage (V_{OC}), 0.50 fill factor (FF), and 4.86% conversion efficiency (η) (Figure 3).

$CH_3NH_3PbI_3$ is bifunctional and can act both as a photoabsorber and a hole conductor.[10] The addition of CuSCN on $CH_3NH_3PbI_3$ improved the photocurrent significantly; Figure 3 shows the change from line (a) to (c) (without hot-air drying) and that from line (b) to (d) (with hot-air drying) by the inclusion of CuSCN. The improvement in the photovoltaic characteristics can be attributed to improved charge separation due to the hole extraction by CuSCN.

Without the CuSCN layer, the photocurrent decreased from 4.6 to 0.83 mA cm^{-2} with decreasing $CH_3NH_3PbI_3$ thickness (from line (a) to (b) in Figure 3 and Table 1). Thus, without a hole-transport material, the volume of the $CH_3NH_3PbI_3$ layer is important for charge separation. However, with the CuSCN hole conductor on $CH_3NH_3PbI_3$, the photocurrent increased

Table 1. Photovoltaic characteristics (from Figure 3) under AM 1.5 (100 mW cm^{-2}). Each result is the average of three cells. The cell size was 25 mm^2 (5 mm × 5 mm).

Lines in Figure 3	Hot-air drying	CuSCN	J_{SC} [mA cm^{-2}]	V_{OC} [V]	FF	η [%]
(a)	without	without	4.6	0.62	0.46	1.35
(b)	with		0.83	0.69	0.40	0.83
(c)	without	with	9.3	0.64	0.33	1.82
(d)	with		14.5	0.63	0.53	4.85

from 9.3 to 14.5 mA cm^{-2} with decreasing $CH_3NH_3PbI_3$ thickness (from line (c) to (d) in Figure 3 and Table 1), and the fill factor was increased, too. Therefore, decreasing the $CH_3NH_3PbI_3$ thickness improves the transportation of accumulated holes[11] into the CuSCN hole conductor, which results in an improvement of the photovoltaic effect.

The slopes at V_{OC} for lines (a) and (c) in Figure 3 were almost the same, which suggests that the solar cells have the same internal series resistance. Although the addition of CuSCN on the thick $CH_3NH_3PbI_3$ layer improved the photocurrent, it did not change the slopes at V_{OC}. Hence, the CuSCN did not decrease the internal series resistance due to the presence of the thick $CH_3NH_3PbI_3$ layer. On the other hand, the CuSCN addition did improve the slope at V_{OC} for the hot-air-dried $CH_3NH_3PbI_3$ layer (from line (b) to (d) in Figure 3). The difference can be attributed to the thin $CH_3NH_3PbI_3$ layer on the nanocrystalline TiO_2 electrode and to the improvement of hole extraction by the addition of CuSCN.

The stability of unencapsulated $CH_3NH_3PbI_3$ solar cells under irradiation at AM 1.5 (100 mW cm^{-2}) was examined in Figure 4. The solar cell with a structure of < FTO/TiO_2/thick $CH_3NH_3PbI_3$ (without hot-air drying)/Au >, which had a thick layer of $CH_3NH_3PbI_3$ without the CuSCN hole-transport layer (line (a) in Figure 4), was unstable. After several minutes, the conversion efficiency deteriorated to 70% of its initial value and slowly decreased to 6% after 16 h. In contrast, the addition of CuSCN onto the thick layer of $CH_3NH_3PbI_3$ improved the stability (line (b) in Figure 4). It was considered that the CuSCN layer may block water to enhance the stability of $CH_3NH_3PbI_3$ as spiro-OMe-TAD or PTAA. Although an initial drop of the efficiency was observed, the cell maintained an efficiency that was about 40% of its initial value. The stability of the cell with the highest efficiency, < FTO/TiO_2/thin $CH_3NH_3PbI_3$ (with hot-air drying)/CuSCN/Au >, was worse (line (c) in Figure 4) than that for the other cells. The conversion efficiency decreased rapidly to 10% of the initial value after 5 h and became zero at 12 h. With hot-air drying during spin coating, the $CH_3NH_3PbI_3$ layer became very thin in the porous TiO_2 layer, which indicates that the thickness of the $CH_3NH_3PbI_3$ layer is important for the stability of $CH_3NH_3PbI_3$ solar cells. Each cell was fabricated and studied for the stability test without a glove box, just under ambient air conditions. The humidity ranged from 30% (fine weather) to 90% (rainy day). As good-efficiency cells have been fabricated on a rainy day, it is considered that the devices are not as sensitive to the humidity as the reported $CH_3NH_3PbI_3$ device using organic hole-transporting materials.

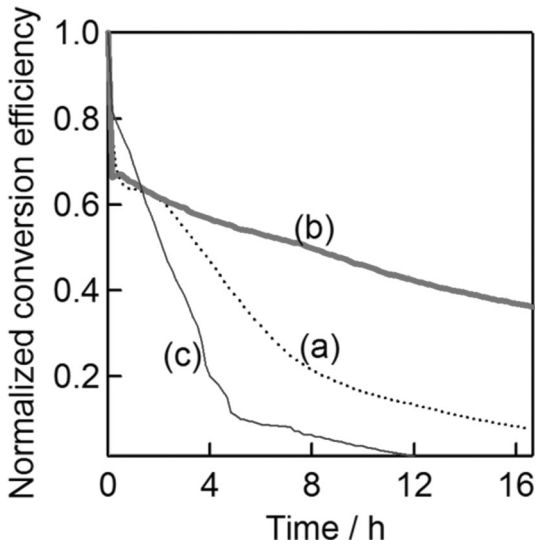

Figure 4. Variation of photovoltaic characteristics for unencapsulated solar cells during light exposure in air: line a) < FTO/TiO_2/$CH_3NH_3PbI_3$ (without hot-air drying)/Au >; b) < FTO/TiO_2/$CH_3NH_3PbI_3$ (without hot-air drying)/CuSCN/Au >; c) < FTO/TiO_2/$CH_3NH_3PbI_3$ (with hot-air drying)/CuSCN/Au >.

During the stability test under irradiation (AM 1.5, 100 mW cm^{-2}) without encapsulation, color variations in the solar cells were observed. Before the stability test, the cells were black (Figure 5a). Without the CuSCN layer or without the thick $CH_3NH_3PbI_3$ layer, the cells became completely yellow after irradiation for 16 h (Figure 5b,d). However, the black color was partially retained (Figure 5b) with the addition of the CuSCN layer onto the thick $CH_3NH_3PbI_3$ layer. The variation in color was consistent with the stability test results shown in Figure 4. Variation in the absorption spectra during the light stability test was confirmed (Figure 6). Before the stability test, the absorption edge was at 800 nm, which is due to the black layer of $CH_3NH_3PbI_3$; however, the absorption edge was shifted to 530 nm after irradiation for 16 h. Although the cells after irradiation for 16 h can absorb light below 530 nm, the photovoltaic characteristics are significantly deteriorated and come close to zero (Figure 4).

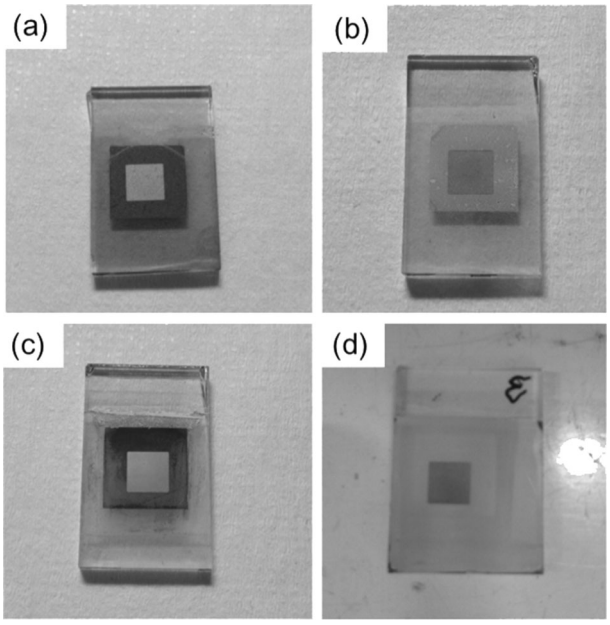

Figure 5. Photographs of < FTO/TiO_2/$CH_3NH_3PbI_3$ (without hot-air drying)/Au > solar cells a) before and b) after light exposure for 16 h, and of c) < FTO/TiO_2/$CH_3NH_3PbI_3$ (without hot-air drying)/CuSCN/Au > and d) < FTO/TiO_2/$CH_3NH_3PbI_3$ (with hot-air drying)/CuSCN/Au > solar cells after light exposure for 16 h.

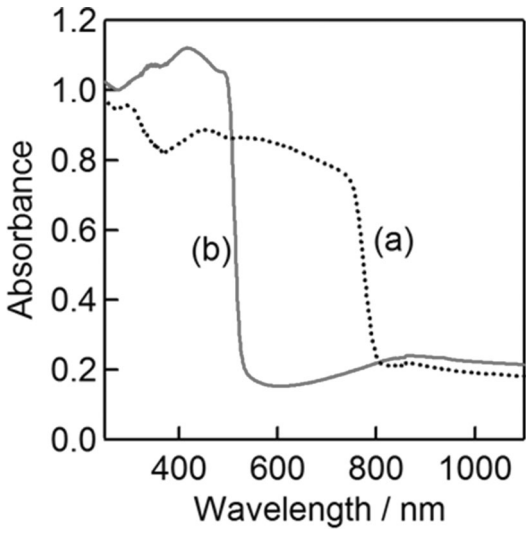

Figure 6. Refractive absorption spectra for nanocrystalline $TiO_2/CH_3NH_3PbI_3$ layers: trace a) before and b) after light exposure (AM 1.5, 100 mW cm^{-2}) for 16 h. The $CH_3NH_3PbI_3$ layers were prepared by spin coating with hot-air drying.

Variation of the structures was also evaluated after the light stability test. Figure 7 shows the X-ray diffraction (XRD) pattern for $CH_3NH_3PbI_3$ on nanocrystalline TiO_2 before and after light exposure without encapsulation, and PbI_2 powder as a reference. Prior to the light exposure, a clear XRD pattern for $CH_3NH_3PbI_3$ was observed.[9] However, after the light exposure, the $CH_3NH_3PbI_3$ peaks disappeared, and the main peak at 14.1° was shifted to 12.8°, which was a small peak in the $CH_3NH_3PbI_3$ pattern before light exposure. The peak at 12.8° is attributed to PbI_2, which is shown as pattern (c) in Figure 7. The XRD peak at 25.5° in pattern (b) of Figure 7 is attributed to TiO_2 (anatase). Therefore, it is concluded that the $CH_3NH_3PbI_3$ perovskite structure was changed to a hexagonal PbI_2 structure due to light exposure without encapsulation.

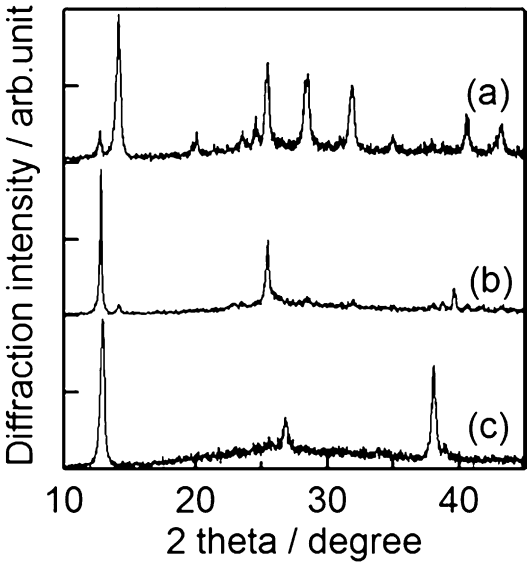

Figure 7. XRD patterns for nanocrystalline $TiO_2/CH_3NH_3PbI_3$ layers: trace a) before and b) after light exposure (AM 1.5, 100 mW cm^{-2}) for 16 h, and c) PbI_2 powder.

The surface morphology of $CH_3NH_3PbI_3$ also changed after light exposure. Prior to light exposure, the surface structure was planar and composed of large round grains covered with rhombohedral crystals (Figure 8a). However, after light exposure the round grains had vanished and the surface appeared more porous between the crystals (Figure 8b). The remaining crystals on the surface were characterized as PbI_2 by XRD measurements (Figure 7).

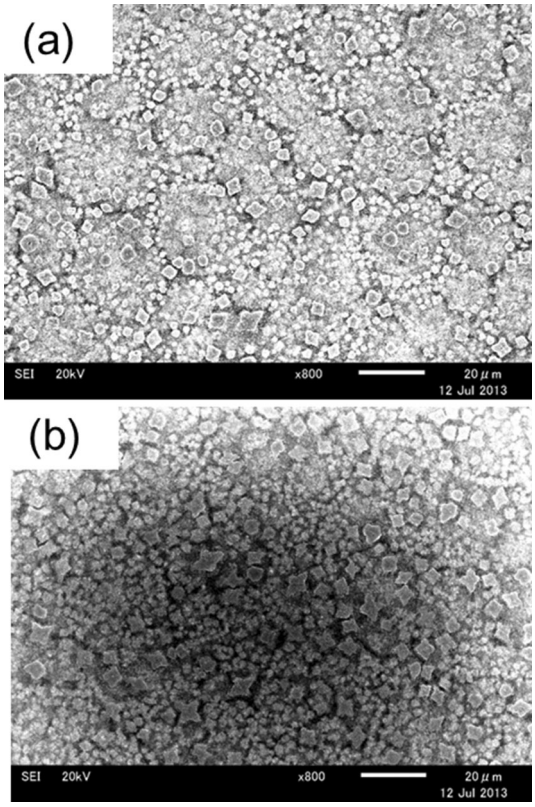

Figure 8. SEM images of nanocrystalline $TiO_2/CH_3NH_3PbI_3$ layers a) before and b) after light exposure (AM 1.5, 100 mW cm^{-2}) for 16 h.

Therefore, it appears that CH_3NH_3I is removed from the $CH_3NH_3PbI_3$ perovskite crystal to leave PbI_2 hexagonal crystals. The $CH_3NH_3^+$ cations are not fixed in the $CH_3NH_3PbI_3$ crystal. Mosconi et al. reported the rotation of $CH_3NH_3^+$ cations in the $CH_3NH_3PbI_3$ perovskite crystal by using density functional theory (DFT) computational simulations,[12] in which the Pb–I bond can form a lattice structure in the $CH_3NH_3PbI_3$ perovskite crystal and $CH_3NH_3^+$ cations can move in the Pb–I lattice. Wasylishen et al. determined the rotation of the $CH_3NH_3^+$ cations in the $CH_3NH_3PbI_3$ perovskite crystals by nuclear magnetic resonance (NMR) experiments.[13] Moreover, Poglitsch and Weber reported the temperature-dependent structure of $CH_3NH_3PbX_3$ (X = Cl, Br, I) determined by XRD measurements, which was compared with measurements of the temperature-dependent complex permittivity at frequencies in the range of 50–150 GHz; it was concluded that a special feature of the

$CH_3NH_3^+$ cation is that it cannot be fixed in the crystal structure.[14] Thus, the non-fixed $CH_3NH_3^+$ cation can move and migrate in the crystal, which explains the loss of CH_3NH_3I from the $CH_3NH_3PbI_3$ crystal by light exposure. X-ray photoelectron spectroscopy (XPS) and Auger electron spectroscopy (AES) measurements were performed to confirm CH_3NH_3I removal; however, no concrete evidence could be obtained. Therefore, further research will be necessary to determine such details.

Electrical impedance spectroscopy (EIS) was used to separate the perovskite $CH_3NH_3PbI_3$ cell resistance into its partial components of series resistance, hole-transport resistance, and recombination resistance. A simple equivalent circuit consisting of two series-connected capacitor–resistor parallel connections in series with the cell series resistance was used (see Figure 9a), as proposed by Boix et al. for ETA cells with CuSCN as

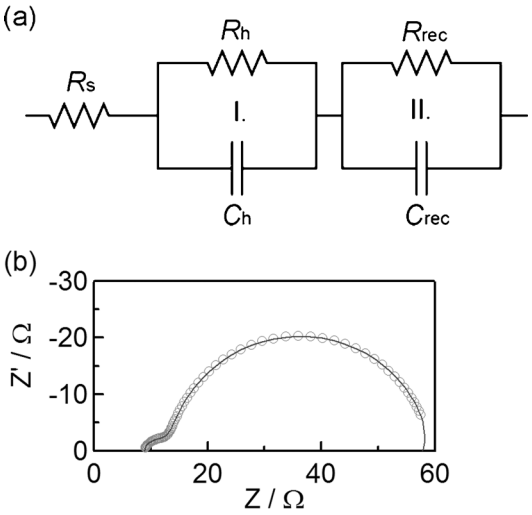

Figure 9. a) Equivalent circuit used for the ETA cell with CuSCN as the hole-transport material. b) Typical Nyquist plot with fitted curve superimposed (white circles: fit results; line: measured data points).

a hole-transport medium.[15] The simple equivalent circuit corresponded well with the measurement data throughout the bias voltage range, and especially well in the mid- to high-bias region. An example of the correspondence between the experimental data and the equivalent circuit fit is shown in Figure 9b, in which the smaller semicircle on the left (I.) corresponds to the EIS response of the hole-transport material and the larger semicircle on the right (II.) is derived from the charge recombination from the TiO_2 layer to the hole-transport material.[15]

The differential hole-transport and recombination resistances determined by the EIS analysis at different bias voltages are shown in Figure 10a and b. The hole-transport resistance of the cells produced without hot air treatment is higher than that of the cells produced with the hot air treatment, throughout the whole bias voltage range applied. This phenomenon can be assigned to the improved penetration of $CH_3NH_3PbI_3$ into the TiO_2 pores when hot air is applied during spin coating. The SEM images in Figure 2b show a thinner layer of

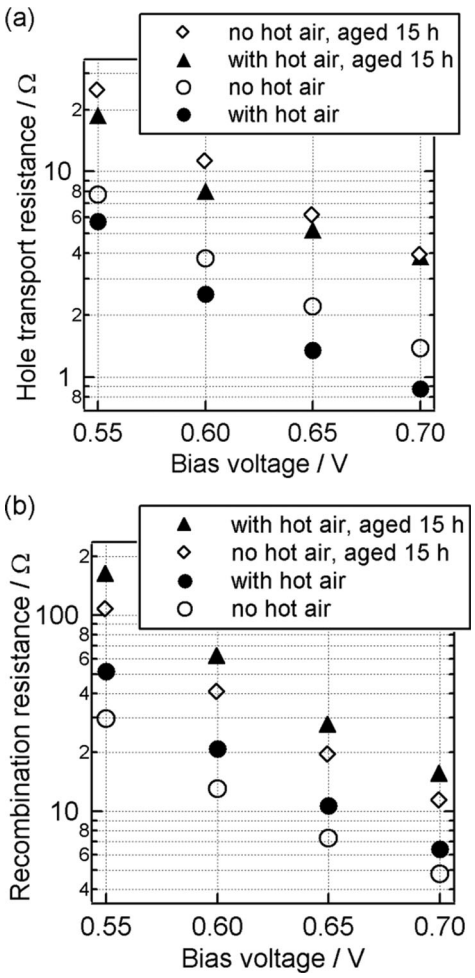

Figure 10. Impedance spectroscopy of $<FTO/TiO_2/CH_3NH_3PbI_3/CuSCN/Au>$ solar cells with and without hot air treatment during the deposition of $CH_3NH_3PbI_3$. a) Hole-transport resistance of the ETA cells before aging with (●) and without (○) hot air treatment, and both cell types after aging for 15 h under 1 Sun (◆ and ◇). b) Recombination resistance of ETA cells before aging with (■) and without (□) hot air treatment, and after aging for 15 h under 1 Sun (▲ and △). EIS of each device was measured in the dark and under short-circuit conditions with nine different bias voltages between 0.55 and 0.70 V. The results represent the average of three different cells.

$CH_3NH_3PbI_3$ between the TiO_2 layer and the back contact. The hole-transport properties for $CH_3NH_3PbI_3$ are poorer than those for CuSCN; therefore, it is beneficial to minimize the thickness of $CH_3NH_3PbI_3$ outside the porous TiO_2 and have only CuSCN filling the interlayer between the TiO_2 layer and the back contact. Figure 10b shows that the recombination resistance in the perovskite $CH_3NH_3PbI_3$ cells produced with hot air treatment is also higher than that in the cells produced without the hot air treatment; however, the reason for this is yet to be determined. Taking these considerations into account, it appears that the improvement of the perovskite $CH_3NH_3PbI_3$ cell conversion efficiency when hot air is employed during $CH_3NH_3PbI_3$ deposition (see Figure 3) is related to the decreased resistance of the hole-transport layer on the one hand, and an increase in the recombination resistance on the other hand.

For the cells of $<FTO/TiO_2/CH_3NH_3PbI_3$ (without hot-air drying)/CuSCN/Au> (in Figure 3c), the initial loss of current at

about 0.2 V may be due to the internal resistance of the thick $CH_3NH_3PbI_3$ outside the porous TiO_2, also. Because of the light degradation of each cell, however, the photocurrent loss cannot be analyzed by impedance spectroscopy precisely, which takes time during the measurements.

The significantly detrimental effect of light exposure on the perovskite $CH_3NH_3PbI_3$ cell conversion efficiency (Figure 4) is also evident in the EIS spectra of these cells. Figure 10a and b shows a half an order of magnitude increase in both the hole-transport resistance and the recombination resistance. This phenomenon can be linked to the change in the crystal structure of the nanocrystalline $TiO_2/CH_3NH_3PbI_3$ layer under light exposure, as shown by the SEM images in Figure 8. Therefore, it can be concluded that this rapid degradation in conversion efficiency under irradiation is due to an increased voltage loss in the hole-transport layer due to light-induced changes in the crystal structure of $CH_3NH_3PbI_3$.

3. Conclusions

$CH_3NH_3PbI_3$ solar cells were fabricated and their structure was changed by using a hot air flow during the spin-coating process. Light exposure tests of the $CH_3NH_3PbI_3$ solar cells without encapsulation were performed for the first time. Although a thin $CH_3NH_3PbI_3$ layer was better for higher photovoltaic effects with the CuSCN hole conductor, a thick $CH_3NH_3PbI_3$ layer with CuSCN was more stable. During the light exposure test without CuSCN, the black $CH_3NH_3PbI_3$ layers were completely changed to yellow, because the perovskite $CH_3NH_3PbI_3$ was changed to hexagonal PbI_2. Therefore, it is concluded that CH_3NH_3I is removed from the $CH_3NH_3PbI_3$ crystal under light exposure. This idea is supported by the non-fixed characteristics of the $CH_3NH_3^+$ cation in $CH_3NH_3PbI_3$ crystals.[12–14] The latest method for $CH_3NH_3PbI_3$ deposition to produce 15.0% solar cells (sequential deposition) involved applying sufficient amounts of CH_3NH_3I during the second deposition,[9] which facilitates the inhibition of photovoltaic deterioration due to the removal of CH_3NH_3I. In this research, in contrast, the loss of $CH_3NH_3PbI_3$ should be considered during the hot-air spin coating, which can be measured by thermogravimetry/differential thermal analysis and FTIR spectroscopy for further investigation. Light exposure tests with encapsulation have shown that $CH_3NH_3PbI_3$ is stable for 500 h.[9] Therefore, if the loss of CH_3NH_3I can be prevented under light irradiation, the stability of $CH_3NH_3PbI_3$ solar cells can be extended.

The effect of the CuSCN coverage against humidity, however, is still not clear. In the results above, the cells of $<$FTO/$TiO_2/CH_3NH_3PbI_3$/CuSCN/Au$>$ did not have strong humidity effects. In contrast, the cells of $<$FTO/$TiO_2/CH_3NH_3PbI_3$/spiro-OMe-TAD (or PTAA)/Au$>$ had strong humidity effects.[8] The difference was just about the hole-transporting material (organic or inorganic). Hence, it was considered that the humidity effect can be mainly attributed to the hole-transporting material (or the interface of the hole-transporting material/$CH_3NH_3PbI_3$) rather than $CH_3NH_3PbI_3$ itself. In the spring 2013 meeting of the Chemical Society of Japan, Shinohara and coworkers (Merck) presented strong humidity effects of lithium salt in the hole-transporting material,[16] which is the same as lithium-ion batteries. On the other hand, Noh et al. reported that the photovoltaic degradation of $CH_3NH_3PbI_3$ cells against humidity was more sensitive than that of $CH_3NH_3PbBr_{2.4}I_{0.6}$.[8] Hence, the photovoltaic degradation against humidity is related to the component of $CH_3NH_3PbX_3$, also. Therefore, the interface of the hole-transporting material/$CH_3NH_3PbI_3$ may deteriorate much faster than CuSCN by humidity. To understand the inside, however, we still need a lot of investigations in the future.

Experimental Section

TiO_2 electrodes were fabricated on F-doped SnO_2 (FTO)-coated glass plates (TEC-15, thickness = 2 mm, NSG-Pilkington). The edge of the FTO layer was first etched using Zn powder and HCl to eliminate shunting of the solar cell at the edge. The etched FTO substrate with detergent was put into an ultrasonic bath, the substrate was rinsed with water and ethanol, and then treated with a UV/O_3 cleaner for 15 min. Dense TiO_2 layers were coated on the FTO by spray pyrolysis using a solution of titanium diisopropoxide bis(acetylacetonate) (TAA; 0.6 mL) in ethanol (9 mL, Kanto Chemical Co., Inc., Japan) on a hot plate at 450 °C. The TAA was prepared by pouring acetylacetone (Wako Pure Chemical Industries, Ltd., Japan) into titanium isopropoxide (Kanto Chemical Co., Inc., Japan) with the ratio of 1:2 (mol/mol).

A nanocrystalline TiO_2 layer was fabricated by screen printing TiO_2 paste that was synthesized by a hydrothermal method under basic conditions and annealed at 550 °C.[17] The thickness of the nanocrystalline TiO_2 layer was approximately 2 μm (see Figure 2).

The $CH_3NH_3PbI_3$ layer was deposited by spin coating under ambient conditions. The $CH_3NH_3PbI_3$ solution was prepared from a mixture of PbI_2 (1.1453 g, Kishida Chemical Co. Ltd., Japan) and CH_3NH_3I (0.395 g) in γ-butyrolactone (2 mL; Kishida Chemical Co. Ltd., Japan). The CH_3NH_3I was synthesized by mixing HI (Tokyo Chemical Industry Co., Ltd., Japan) and CH_3NH_2 (Tokyo Chemical Industry Co., Ltd., Japan) according to ref. [10]. $CH_3NH_3PbI_3$ solution (40 μL) was dropped on the porous TiO_2 layer and spin-coated at 2000 rpm for 30 s. The acceleration was 667 rpm s^{-1}. During the spin coating, hot air from a hair drier was applied to the substrate. The temperature of the TiO_2 electrode during the hot-air blowing was 70–80 °C, checked by thermography (THI-502B-1, FLIR). After the deposition of $CH_3NH_3PbI_3$, the substrate was annealed at 100 °C for 15 min under a N_2 flow. CuSCN (Kishida Chemical Co. Ltd., Japan) layers and Au back contacts were deposited using the doctor-blade process and vacuum evaporation, respectively.[2,3]

Scanning electron microscopy (SEM; JSM-6510, JEOL) was employed to evaluate the morphology of the films. The crystal structure was characterized using X-ray diffraction (XRD; Miniflex II, Rigaku) with CuKα radiation. UV/Vis absorption spectra were measured using a UV/Vis spectrometer (Lambda 750, PerkinElmer). The size of the samples used for photocurrent–voltage (*I–V*) measurements was 25 mm^2 (5 mm × 5 mm). Photovoltaic measurements employed an AM 1.5 solar simulator equipped with a 500 W Xe lamp (YSS-80A, Yamashita Denso). The power of the solar simulator light was calibrated to 100 mW cm^{-2} using a reference Si photodiode (Bunkou Keiki). *I–V* curves were obtained by application of an external bias to the cell and measurement of the generated photocurrent with a DC voltage current source (6240, ADCMT). The differential hole-transport resistance and recombination resistance

were determined by electrical impedance spectroscopy (EIS) measurements in the dark at various bias voltages between 0.55 and 0.70 V. The EIS spectra were measured using a potentiostat (SP-150, Bio-Logic). Zview2 software was used for the fitting. The differential resistances given represent the average for three different cells.

Acknowledgements

This work was supported by the Advanced Low Carbon Technology Research and Development Program (ALCA) of the Japan Science and Technology Agency (JST).

Keywords: energy conversion · hole transport · perovskite phases · solar cells · structure control

[1] R. T. Morrison, R. N. Boyd in *Organic Chemistry, 6th ed.*, **1992,** Prentice-Hall, Inc., A Simon and Schuster Company, Englewood Cliffs, New Jersey 07632.
[2] K. Tsujimoto, D.-C. Nguyen, S. Ito, H. Nishino, H. Matsuyoshi, A. Konno, G. R. A. Kumara, K. Tennakone, *J. Phys. Chem. C* **2012**, *116*, 13465 – 13471.
[3] S. Ito, K. Tsujimoto, D.-C. Nguyen, K. Manabe, H. Nishino, *Int. J. Hydrogen Energy* **2013**, *38*, 16749 – 16754.
[4] D.-C. Nguyen, Y. Mikami, K. Tsujimoto, T. Ryo, S. Ito, *Jpn. J. Appl. Phys.* **2012**, *51*, 10NC23.
[5] D.-C. Nguyen, S. Tanaka, H. Nishino, K. Manabe, S. Ito, *Nanoscale Res. Lett.* **2013**, *8*, 8.
[6] H. S. Kim, C. R. Lee, J. H. Im, K. B. Lee, T. Moehl, A. Marchioro, S. J. Moon, R. Humphry-Baker, J. H. Yum, J. E. Moser, M. Grätzel, N. G. Park, *Sci. Rep.* **2012**, *2*, 591.
[7] M. M. Lee, J. Teuscher, T. Miyasaka, T. N. Murakami, H. J. Snaith, *Science* **2012**, *338*, 643 – 647.
[8] J. H. Noh, S. H. Im, J. H. Heo, T. N. Mandal, S. I. Seok, *Nano Lett.* **2013**, *13*, 1764 – 1769.
[9] J. Burschka, N. Pellet, S. J. Moon, R. Humphry-Baker, P. Gao, M. K. Nazeeruddin, M. Grätzel, *Nature* **2013**, *499*, 316 – 319.
[10] L. Etgar, P. Gao, Z. Xue, Q. Peng, A. K. Chandiran, B. Liu, M. K. Nazeeruddin, M. Grätzel, *J. Am. Chem. Soc.* **2012**, *134*, 17396 – 17399.
[11] H. S. Kim, I. Mora-Sero, V. Gonzalez-Pedro, F. Fabregat-Santiago, E. J. Juarez-Perez, N. G. Park, J. Bisquert, *Nat. Commun.* **2013**, *4*, 2242.
[12] E. Mosconi, A. Amat, M. K. Nazeeruddin, M. Grätzel, F. De Angelis, *J. Phys. Chem. C* **2013**, *117*, 13902 – 13913.
[13] R. E. Wasylishen, O. Knop, J. B. Macdonald, *Solid State Commun.* **1985**, *56*, 581 – 582.
[14] A. Poglitsch, D. Weber, *J. Chem. Phys.* **1987**, *87*, 6373 – 6378.
[15] P. P. Boix, G. Larramona, A. Jacob, B. Delatouche, I. Mora-Seró, J. Bisquert, *J. Phys. Chem. C* **2012**, *116*, 1579 – 1587.
[16] H. Shinohara, Y. Shawada, S. Renker (Merck), "Development of materials for solid-state dye-sensitized solar cells", *ATP session (T1) in the spring meeting of the Chemical Society of Japan* (24th March, Ritsumeikan University, Shiga, Japan) **2013**, 3H1 – 28.
[17] S. Ito, S. M. Zakeeruddin, P. Comte, P. Liska, D. Kuang, M. Grätzel, *Nat. Photonics* **2008**, *2*, 693 – 698.

Received: November 11, 2013
Revised: February 1, 2014
Published online on ■■ ■■, 2014

S. Ito, S. Tanaka, H. Vahlman, H. Nishino, K. Manabe, P. Lund*

■■ – ■■

Carbon-Double-Bond-Free Printed Solar Cells from $TiO_2/CH_3NH_3PbI_3$/CuSCN/Au: Structural Control and Photoaging Effects

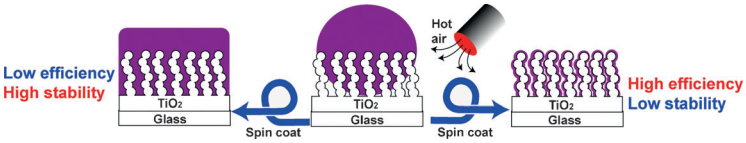

It's all hot air! Solar cells are fabricated from Pb perovskite ($CH_3NH_3PbI_3$) and CuSCN. The thickness of the $CH_3NH_3PbI_3$ layer is controlled by a hot air flow during spin coating (see figure). Although the best conversion efficiency (4.86%) is obtained with a thin $CH_3NH_3PbI_3$ layer, a thick $CH_3NH_3PbI_3$ layer is better for light-exposure stability.